Comparison of SEB Cross-section between Spallation Neutron and Mono-energetic Proton for SiC MOSFETs

Chao Peng*, Zhifeng Lei, Zhangang Zhang, Teng Ma, Hong Zhang, Yujuan He, Yun Huang

Science and Technology on Reliability Physics and Application of Electronic Component Laboratory, China Electronic Product Reliability and Environmental Testing Research Institute, Guangzhou, 511370, China

Abstract: The radiation-induced single event burnout (SEB) is observed for SiC MOSFETs by conducting proton and spallation neutron irradiation. Proton irradiation at different energies indicates that the SEB cross-section increases with the increase of proton energy. Under different bias voltages, the SEB cross-section of protons with energies of 100 MeV and above will exceed that of spallation neutrons. The atmospheric neutron SEB failure rates of SiC MOSFETs are calculated based on the proton-induced and neutron-induced SEB cross-sections, respectively. The failure rates calculated by the two different methods are consistent, with the error between the two results being less than 49%. The information of the secondary ions produced by spallation neutron and proton is obtained through Monte Carlo simulations. The simulation results imply that the SEB caused by protons and spallation neutrons is strongly correlated with the ionizing energy deposition of their secondary ions from nuclear reactions. As the proton energy increases, the number of secondary ion products with sufficient energy deposition to induce SEB increases. The magnitude of the SEB cross-sections for spallation neutrons and protons also depends on the number of secondary particles that deposit energy above the threshold energy.

Keywords: Atmospheric neutron failure rate, SiC MOSFET, singe event burnout, spallation neutron

1. Introduction

The advantages of SiC power MOSFET, such as high efficiency, high voltage tolerance, and low loss, have enabled their widespread application in fields like new energy vehicles, charging piles, and photovoltaics [1],[2]. Power devices used in terrestrial applications face the risk of failure due to atmospheric neutron. The previous studies had proved that power electronic devices are vulnerable to terrestrial cosmic radiation [3]-[5]. SiC MOSFETs also have the above-mentioned reliability issues. A large number of literatures had reported the destructive failure of single event burnout (SEB) caused by atmospheric neutrons [6]-[10]. Atmospheric neutron-induced SEB is one of the most serious reliability problems for SiC MOSFETs in the terrestrial applications [11]. Therefore, in order to meet the high reliability requirements of SiC MOSFETs in power applications, it is necessary to evaluate the failure rate caused by atmospheric neutrons.

The most effective way to estimate the atmospheric neutron failure rate is to carry out accelerated irradiation test. JEDEC JEP151 standard had suggested that two types of nucleon beams can be used for accelerating test of power devices: mono-energetic proton and spallation neutron [12]. Spallation neutrons are an ideal radiation source because their energy spectrum approximates that of natural atmospheric neutrons. If mono-energetic protons are employed for the accelerated testing, the energy should be at least 150 MeV. Due to the difference in energy spectra, a mono-energetic proton beam of at least 150 MeV cannot reflect the effects of low energy portion of the natural atmospheric spectrum.

Corresponding authors: pengchaoceprei@qq.com

This work was supported in part by the National Natural Science Foundation of China under Grants 12375268, the Guangzhou Science and Technology Program Project under Grant 2025A04J2781, the Guangdong Basic and Applied Basic Research Foundation under Grant 2022A1515111049.

Therefore, it may overestimate the device failure rate due to terrestrial atmospheric neutron. JEDEC JESD89A standard had pointed out that the atmospheric neutron-induced soft error of SRAM can be obtained by the Weibull fits to the mono-energetic proton SEU cross section data [13],[14]. Perhaps the Weibull fitting curves of the SEB cross-sections of protons with different energies can also be used to assess the atmospheric neutron failure rate of power devices. However, this method has not been verified by experiment and the applicability of this method to power devices is still uncertain.

In this paper, irradiation tests with spallation neutrons and mono-energetic protons of different energies are conducted for SiC MOSFETs. The differences in SEB cross-sections between spallation neutrons and protons of different energies are compared. Then, the atmospheric neutron failure rates of SiC MOSFETs are calculated based on the accelerated test results from the two different radiation sources. Finally, secondary ion characteristics obtained through Monte Carlo simulation are used to explain the differences in SEB cross-sections between spallation neutrons and protons.

2. Experimental details

The commercially available SiC n-channel power MOSFETs C3M0065090D (900 V, 36A, 65 mΩ) from CREE Inc. were used as experimental samples. Since the high energy proton and neutron can penetrate the package materials, the samples were irradiated from the front side without removing packages. The 40~100 MeV proton irradiations were conducted at Northwest Institute of Nuclear Technology. The flux is 1×10^8 p/cm^2/s for 40 MeV proton and is 2×10^7 p/cm^2/s for the other energies. The 200 MeV and 300 MeV proton irradiations were conducted at the Space Environment Simulation and Research Infrastructure (SESRI) in Harbin Institute of Technology. The average proton flux is 5×10^6 p/cm^2/s. During proton irradiations, the test boards were mounted on a two-dimension-movement platform and only one sample was irradiated at one time, as shown in Fig. 1 (a). The proton beam area is 2 cm$\times$2 cm and it can cover the active area of the device. The DUT was aligned to the center of the proton beam by laser. The proton beam was at normal incidence. The devices were OFF biased during irradiation, i.e. drain terminal biased at a positive high voltage, source and gate grounded. The drain terminal of the device was biased by a Keithley 2290 high voltage power supply, as shown in Fig. 1 (b). The drain current is real-time monitored by a Keithley DMM7510 multi-meter during irradiation. The multi-meter has an internal resistance of 10 MΩ in series with the device under test (DUT). The real-time monitored current will be limited by this internal resistance when the DUT is burnout. The irradiation experiments were conducted at different operating voltages and three samples are tested for each voltage.

Neutron irradiations were conducted using Atmospheric Neutron Irradiation Spectrometer (ANIS) at the China Spallation Neutron Source (CSNS). The energy spectrum of this spallation neutron spectrum is presented in our previous published works [15],[16]. The maximum neutron energy is above 1 GeV and the neutron flux at the sample location with energy above 10 MeV is 6.17×10^5 n/cm^2/s. The test setup for spallation neutron irradiation is same as that in [16]. The neutron irradiation experiments were also conducted at different operating voltages and ten samples were tested at each voltage. The beam is at normal incidence and the beam area is 10 cm$\times$6 cm. All the ten samples could be irradiated at the same time. The irradiation under a specific voltage was finished, when all devices were fail or the total neutron fluence (>10 MeV) was up to 9×10^9 n/cm^2.

3. Results and discussions

A. SEB cross-section and failure rate calculations under different radiation source

Fig. 2 shows the real-time monitored currents of the multi-meter during proton irradiation when the SiC MOSFET is biased at 750 V. There is a proton pulse incident into the device every 12 s. A transient current pulse is observed accompanied by the incidence of a proton pulse. A SEB event occurs when the total proton fluence is up to 7.28×10^{8} /cm^2. It is manifested as an abrupt increase of drain current. The SEB damage regions in SiC MOSFET are located by Emission Microscope (EMMI) test and the emission region indicates the location of the damage, as shown in Fig. 3. The damage regions are randomly distributed. Fig. 3 also show the SEM image of the damage region. The material has melted due to the thermal runaway in the SEB. The similar SEB phenomenon is also observed under spallation neutron irradiation [15].

SEB cross-sections corresponding to different drain bias voltages under mono-energetic proton irradiation for the 900 V SiC MOSFETs are calculated by:

$$\sigma_{SEB,proton}(E_p, V_{bias}) = \frac{r}{\phi_{proton}} \tag{1}$$

where E_p is the proton energy, V_{bias} is the drain bias voltage during irradiation, r is the total number of failures under irradiation with V_{bias}, ϕ_{proton} is the sum of the proton fluence for each irradiated device. The calculated SEB cross-sections results are shown in Tab. 1. The relationship between SEB cross-section and proton energy can be obtained by fitting the calculated SEB cross-section data with a four parameter Weibull distribution, which is,

$$\sigma_{SEB,proton}(E_p) = \sigma_0(1-\exp\{-[(E_p - E_0)/W]^S\}) \tag{2}$$

where σ_0 is the saturate SEB cross-section, E_0 is the threshold proton energy, which means that the SEB cross-section can be considered as 0 below this energy, W and S are fitting parameter. The Weibull fitting parameters corresponding to different drain biases are shown in Tab. 2.

Similarly, the SEB cross-sections as a function of drain biases for SiC MOSFETs can also be calculated based on the spallation neutron experimental results,

$$\overline{\sigma_{SEB,neutron}}(V_{bias}) = \frac{r}{\phi_{neutron}} \tag{3}$$

where $\phi_{neutron}$ is the sum of the neutron fluence with energy >10 MeV for each irradiated device. Since the spallation neutrons are neutrons with a continuous energy spectrum, the SEB cross-section obtained in the experiment is the average cross-section caused by neutrons of different energies.

Fig. 4 shows the comparison of SEB cross-section between mono-energetic proton and spallation neutron under different drain biases for SiC MOSFETs. The proton-induced SEB cross-section increase with the drain bias and proton energy. The SEB is only observed for proton irradiation with energies of 60 MeV and above, when the drain bias is below 850 V. When the drain bias is 700 V, the SEB cross-section increase from 5.02×10^{-11} cm^2 to 5.12×10^{-10} cm^2 as the proton energy increase from 60 MeV to 300 MeV. When the drain bias is 850 V, the SEB cross-section increase from 7.86×10^{-12} cm^2 to 7.37×10^{-9} cm^2 as the proton energy increase from 40 MeV to 300 MeV. The average SEB

cross-section caused by spallation neutrons also increases with the increase of drain bias. It is worth noting that when the proton energy is greater than 100 MeV, the corresponding SEB cross-section will exceed the average SEB cross-section caused by spallation neutrons with a bias of 700~850 V. This means that using the proton SEB cross-section at a single energy point above 100 MeV instead of the average spallation neutron cross-section to calculate the atmospheric neutron failure rate would overestimate the failure rate of this SiC device.

Combining the Weibull fitting curve of mono-energetic proton SEB cross-section data and the atmospheric neutron spectrum data, the atmospheric neutron-induced SEB failure rate of the SiC MOSFET can be calculated by,

$$\lambda_{SEB,proton} = \int_{E_{min}}^{E_{max}} dE \left(d\Phi_n(E_n)/dE_n\right)\sigma_{SEB,proton}(E_p) \quad (4)$$

where $d\Phi_n(E_n)/dE_n$ is the differential neutron flux at New York sea level, as shown in Fig. 5, E_{max} and E_{min} are the upper and lower limits of the neutron energy. The calculated SEB failure rates operating at sea level in New York are shown in Tab. 3. The atmospheric neutron-induced SEB rates increase with the applied drain bias. The SEB failure rates are about 2.73 FIT at V_{ds}=700 V and 52.0 FIT at V_{ds}=850 V.

The SEB failure rates of SiC MOSFETs are also calculated based on the spallation neutron SEB cross-section [12],

$$\lambda_{SEB,neutron} = \overline{\sigma_{SEB,neutron}} \times \Phi_n \quad (5)$$

where Φ_n=13 n/cm^2/h is the natural atmospheric neutron flux with energy >10 MeV at New York sea level. The SEB failure rate calculated based on the spallation neutron experiment ($\lambda_{SEB,neutron}$) is consistent with the SEB failure rate calculated based on the proton cross-section ($\lambda_{SEB,proton}$). The maximum error between $\lambda_{SEB,neutron}$ and $\lambda_{SEB,proton}$ is about 49.0%, as shown in Tab. 3.

B. *Comparison of secondary ion characteristics generated by proton and neutron*

Since both neutron and proton causes a SEB through secondary ions generated by nuclear reactions, the different SEB cross-section between mono-energetic proton and spallation neutron can be analyzed by comparing the differences in secondary ion products. The secondary ion products of mono-energetic proton and spallation neutron in SiC MOSFET are obtained by PHITS calculations [17],[18]. The calculation setup is the same as that in our previous published work [15]. A sensitive volume (SV) is defined in the simulation structure. The information of secondary ions generated by nuclear reaction that enter the SV is recorded, since only the energy deposit of secondary ions in SV can contribute to the SEB. According to [19], the sensitive volume for triggering SEB is near the n-drift/n+ drain junction for short-range secondary ions. So a SV with size of 2.5 μm×4 μm×20 μm is defined near the n- drift/n+ drain junction of SiC MOSFET in the PHITS simulation. The mono-energetic neutrons and spallation neutron are incident vertically from the top of the simulation structure. The energies of the incident proton are set as 40 MeV, 60 MeV, 100 MeV, 200 MeV, and 300 MeV. The energy spectrum of the incident spallation neutrons is similar as that in Fig. 5. The total number of incident particles is 5×10^8 for each radiation source.

Fig. 6 (a) shows the number of secondary ions produced by 300 MeV proton and spallation neutron. The secondary ion products cover all ions from H to Si. The total number of secondary ions produced by spallation neutrons is higher than that produced by 300 MeV protons, especially for secondary C, Mg, Al, and Si ions. The maximum energy of the secondary ion (without considering secondary protons) produced by 300 MeV proton and spallation neutron can reach 185 MeV and 139 MeV, respectively. While, 95.2% of the secondary ion produced by spallation neutron has an energy below 10 MeV, and this proportion of the secondary ion produced by 300 MeV proton is 82.2%. Secondary ions mainly induce SEB through ionizing energy deposition. Fig. 7 shows the variation of ionizing energy loss with energy for different secondary ions in the energy range of 0.1 MeV to 200 MeV. The ionizing energy loss is calculated by SRIM code [20]. It can be seen that for energies below approximately 10 MeV, the ionization energy loss of the most secondary ions increases with increasing energy. Due to the low ionization energy loss, secondary ions with low energy are unlikely to induce SEB. If only secondary ions with energies above 2 MeV are considered, then the number of secondary ion products from 300 MeV protons will exceed that of spallation neutrons, as shown in Fig. 6 (b). It means that 300 MeV protons are more likely to induce SEB in SiC MOSFETs. This can explain why SiC devices have a higher SEB cross-section under 300 MeV proton irradiation.

Fig. 8 (a) shows the deposit energies of different secondary ions in the SV of SiC MOSFET for 300 MeV proton. The deposit ionizing energies in SV distribute in the range of 10^{-5}~15.7 MeV. A threshold energy of 2.4 MeV is defined in this work according to the previous heavy ion experimental data [21],[22] of SiC MOSFET. It is assumed that the SEB will occur when the ionizing energy deposition in SV is greater than the threshold energy. In the range of 10^{-5}~0.6 MeV, the total deposit energy in SV mainly comes from the direct ionization of incident protons (H ions). Since the energy depositions in SV of most protons are lower than 1 MeV, it is unlikely to trigger SEB. In the range where energy deposition exceeds 2.4 MeV, the number of He, C, N, O, Ne, Mg ions are relatively high. It implies that these ions are the great contributors to SEB. For the secondary ion products of spallation neutrons, among the ions with energy deposition exceeding 2.4 MeV, He, C, and Mg ions are the most abundant, as shown in Fig. 8 (b). Therefore, these ions are more likely to cause SEB.

Fig. 8 (c) shows the numbers of secondary ions produced by protons with different energies and spallation neutron as a function of deposit energy in SV. For protons with energies of 60 MeV, 100 MeV, 200 MeV, and 300 MeV, the number of secondary ions with energy deposition exceeding 2.4 MeV is 7.26×10^{-7} /source, 9.16×10^{-7} /source, 1.02×10^{-6} /source, and 1.18×10^{-6} /source, respectively. The higher the proton energy, more secondary ions are generated by nuclear reaction. It means that the higher energy protons are more like to cause SEB. This is consistent with the experimental results in Fig. 4 that higher-energy protons have a higher SEB cross-section. At the same time, it can be found that the number of secondary ions with energy deposition exceeding 2.4 MeV is 6.24×10^{-7} /source for spallation neutron, which is lower than that for 60 MeV proton. When the drain bias is closed to the rated voltage, the threshold energy is relatively low (2.4 MeV). The SEB cross-section of spallation neutron is lower than that of 60 MeV proton. This is the situation for V_{bias} of 850 V, as shown in Fig. 4. It is worth to note that the threshold energy will increase with the decrease of drain bias. If the threshold energy is increased to 6.4 MeV, the number of secondary ions with energy deposition exceeding the threshold energy is 1.80×10^{-8} /source, 5.40×10^{-8} /source, 1.26×10^{-7} /source, 1.64×10^{-7} /source, and 3.00×10^{-8} /source for 60~300 MeV protons and spallation neutrons, respectively. The SEB

cross-section of spallation neutron is larger than that of 60 MeV proton, but lower than that of 100 MeV. This is the situation for V_{bias} of 700 V.

4. Conclusion

The mono-energetic protons and spallation neutrons-induced SEB in SiC MOSFETs are investigated. The SEB phenomenon is observed for SiC MOSFET during both proton and spallation neutron irradiation. The proton-induced SEB cross-section increases with the drain bias and proton energy. When the proton energy is increased to 100 MeV, the corresponding SEB cross-section becomes higher than that of spallation neutrons. The atmospheric neutron SEB failure rates at New York sea level are calculated based on the results of accelerated irradiation test using mono-energetic protons and spallation neutrons, respectively. The failure rates are calculated to be 2.73~52.0 FIT corresponding to V_{ds}=700~850V utilizing the results from proton experiments conducted at four distinct energy levels. The failure rates are calculated to be 1.47~26.5 FIT corresponding to V_{ds}=700~850V based on the spallation neutron results. The maximum error between the failure rates calculated by the two methods is 49%. It indicates that both of the aforementioned methods can be employed to assess the atmospheric neutron failure rate of SiC MOSFETs.

The characteristics of secondary ions generated by protons with different energies and spallation neutrons are compared by PHITS simulations. The simulation results indicate that the SEB caused by protons and neutrons is strongly correlated with the ionizing energy deposition of their secondary ions from nuclear reactions. As the proton energy increases, the number of secondary ion products with sufficient energy deposition to induce SEB also increases. Therefore, the SEB cross-section corresponding to higher-energy protons is also higher. When the SiC MOSFET is biased near its rated voltage, the number of secondary ion products from 60 MeV protons that are sufficient to induce SEB is higher than that from spallation neutrons. So the SEB cross-section of spallation neutrons is even lower than that of 60 MeV protons. As the bias voltage of the SiC device decreases, the energy deposition required to induce SEB increases. At this point, the number of secondary ion products from 60 MeV protons that are sufficient to induce SEB will be lower than that from spallation neutrons. Consequently, the average SEB cross-section of spallation neutrons is higher than that of 60 MeV protons.

Acknowledgment

The neutron irradiation beam time was provided by the China Spallation Neutron Source. The author would like to thank for their technical support and help.

References

[1] L. D. Stevanovic, K. S. Matocha, P. A. Losee, J. S. Glaser, J. J. Nasadoski, and S. D. Arthur, “Recent advances in silicon carbide MOSFET power devices,” present at *Twenty-Fifth Annual IEEE Applied Power Electronics Conference and Exposition (APEC)*, pp. 401-407, 2010.

[2] J. Wang, and X. Jiang, "Review and analysis of SiC MOSFETs' ruggedness and reliability," *IET Power Electronics,* vol. 13, no. 3, pp. 445-455, 2020.

[3] C. Peng, L. Yang, Z. Lei, Y. Zhou, T. Ma, Z. Yuan, Z. Zhang, Y. He, and Y. Huang, "Atmospheric neutron-induced single event burnout characterization of 4.5 kV Si IGBTs with spallation neutron irradiation," *Semicond. Sci. Technol.*, vol. 39, Art. no. 085011, 2015.

[4] T. Shoji, H. Tadano, S. Nishida, and K. Hamada, "Cosmic ray neutron-induced single-event burnout in power devices," *IET Power Electronics*, vol. 8, pp. 2315-2321, 2015.

[5] A. Hands, P. Morris, K. Ryden, C. Dyer, P. Truscott, A. Chugg, and S. Parker, " Single event effects in power MOSFETs due to atmospheric and thermal neutrons," *IEEE Trans. Nucl. Sci.,* vol. 58, no. 6, pp. 2687-2694, 2011.

[6] T. Shoji, S. Nishida, K. Hamada, and H. Tadano, "Experimental and simulation studies of neutron-induced single-event burnout in SiC power diodes," *Jap. J. Appl. Phys.*, vol. 53, 04EP03, pp. 1-8, 2014.

[7] A. Akturk, J. M. McGarrity, N. Goldsman, D. Lichtenwalner, B. Hull, D. Grider, and R. Wilkins, "Terrestrial neutron-induced failures in silicon carbide power MOSFETs and diodes," *IEEE Trans. Nucl. Sci.*, vol. 65, no. 6, pp. 1248-1254, 2018.

[8] A. Akturk, R. Wilkins, J. M. McGarrity, and B. Gersey, "Single event effects in Si and SiC power MOSFETs due to terrestrial neutrons," *IEEE Trans. Nucl. Sci.*, vol. 64, no. 1, pp. 529-535, 2017.

[9] C. Martinella, S. Race, R. Stark, R. G. Alia, A. Javanainen, and U. Grossner, "High-energy proton and atmospheric-neutron irradiations of SiC power MOSFETs: SEB study and impact on channel and drift resistances," *IEEE Trans. Nucl. Sci.*, vol. 70, no. 8, pp. 1844-1851, 2023.

[10] H. Asai, I. Nashiyama, K. Sugimoto, K. Shiba, Y. Sakaide, Y. Ishimaru, Y. Okazaki, K. Noguchi, and T. Morimura, "Tolerance against terrestrial neutron-induced single-event burnout in SiC MOSFETs," *IEEE Trans. Nucl. Sci.*, vol. 61, no. 6, pp. 3109-3114, 2014.

[11] C. Martinella, R. G. Alia, R. Stark, A. Coronetti, C. Cazzaniga, M. Kastriotou , Y. Kadi, R. Gaillard, U. Grossner, and A. Javanainen, "Impact of terrestrial neutrons on the reliability of SiC VD-MOSFET technologies," *IEEE Trans. Nucl. Sci.*, vol. 68, no. 5, pp. 634-641, 2021.

[12] JEDEC JEP151 standard, “Test procedure for the measurement of terrestrial cosmic ray induced destructive effects in power semiconductor devices”, 2015.

[13] JEDEC JESD89A standard, “Measurement and reporting of alpha particle and terrestrial cosmic ray-induced soft errors in semiconductor devices”, 2006.

[14] E. L. Petersen, J. C. Pickel, J. H. Adams, and E. C. Smith, "Rate prediction for single event effects-a critique," *IEEE Trans. Nucl. Sci.*, vol. 39, no. 6, pp. 1577-1599, 1992.

[15] C. Peng, Z., Z. Zhang, Y. He, T. Ma, and Yun Huang, "Terrestrial neutron induced failure rate measurement of SiC MOSFETs using China spallation neutron source," *Nucl. Inst. Meth. Phys. Res. B*, vol. 540, pp. 129-135, 2023.

[16] C. Peng, Z. Lei, Z. Zhang, Y. He, T. Ma, Z. Cai, and Y. Chen, "Influence of temperature on atmospheric neutron-induced SEB failure rate for SiC MOSFETs," *IEEE Trans. Nucl. Sci.*, vol. 71, no. 2, pp. 160-166, 2024.

[17] T. Sato, Y. Iwamoto, S. Hashimoto, T. Ogawa, T. Furuta, S. Abe, and et al, "Features of particle and heavy ion transport code system (PHITS) version 3.02," *J. Nucl. Sci. Technol.*, vol. 55, pp. 684-690, 2018.

[18] https://phits.jaea.go.jp.

[19] D. R. Ball, B. D. Sierawski, K. F. Galloway, R. A. Johnson, M. L. Alles, A. L. Sternberg, A. F. Witulski, R. A. Reed, R. D. Schrimpf, A. Javanainen, and J. M. Lauenstein, "Estimating terrestrial neutron-induced SEB cross sections and FIT rates for high-voltage SiC power MOSFETs," *IEEE Trans. Nucl. Sci.*, vol. 66, no. 1, pp. 337-343, 2019.

[20] J. F. Ziegler, M. D. Ziegler, and J. P. Biersack, "SRIM-The stopping and range of ions in matter," *Nucl. Instrum. Meth. Phys. Res. B*, vol. 268, nos. 11-12, pp. 1818-1823, 2010.

[21] E. Mizuta, S. Kuboyama, H. Abe, Y. Iwata, and T. Tamura, "Investigation of single-event damages on silicon carbide (SiC) power MOSFETs," *IEEE Trans. Nucl. Sci.*, vol. 61, pp. 1924-1928, 2014.

[22] A. F. Witulski, D. R. Ball, K. F. Galloway, A. Javanainen, Jean-Marie, Lauenstein, A. L. Sternberg, and R. D. Schrimpf, "Single-event burnout mechanisms in SiC power MOSFETs," *IEEE Trans. Nucl. Sci.*, vol. 65, no. 8, pp. 1951-1955, 2018.

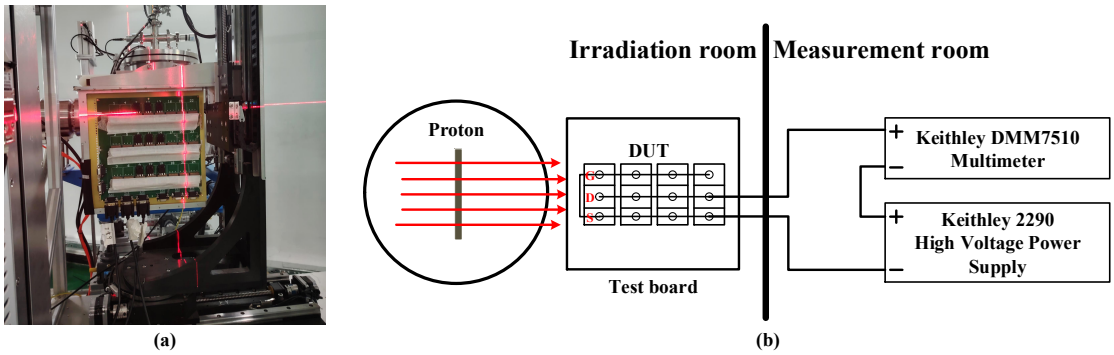

Fig. 1. (a) Test board and sample installation. (b) Test setup for proton irradiation.

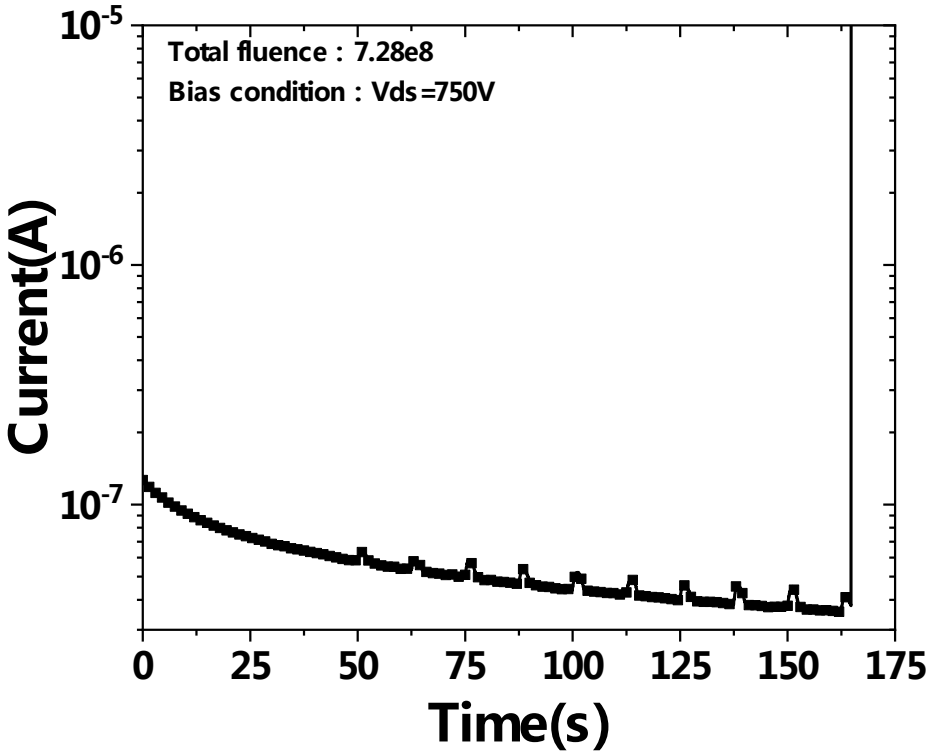

Fig. 2. Current monitored during proton irradiation for 900 V SiC MOSFETs. Bias condition during irradiation: V_{ds}=750 V.

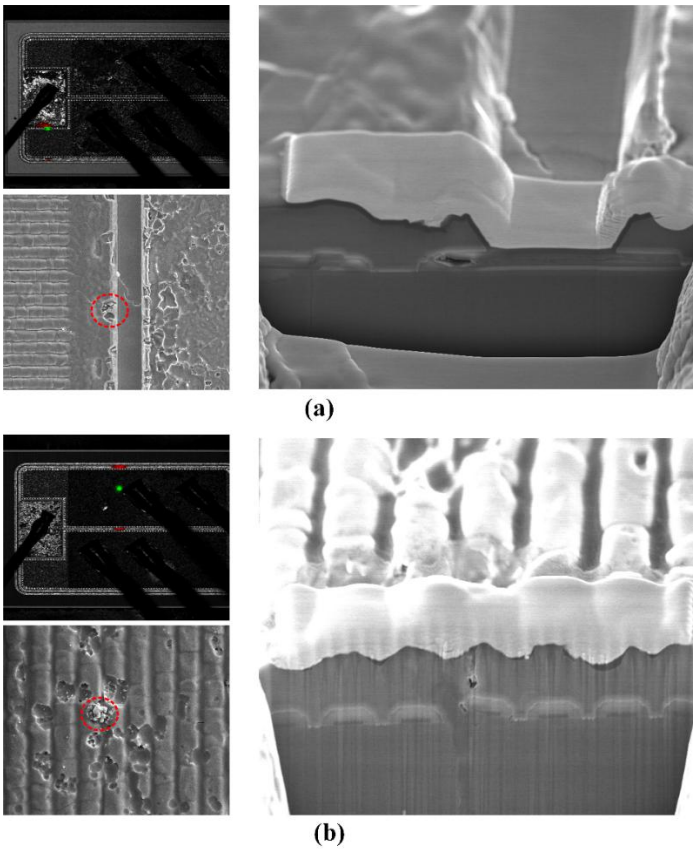

Fig. 3. Damage location and morphology of SiC MOSFETs after irradiation. (a) 200 MeV proton irradiation. (b) 300 MeV proton irradiation.

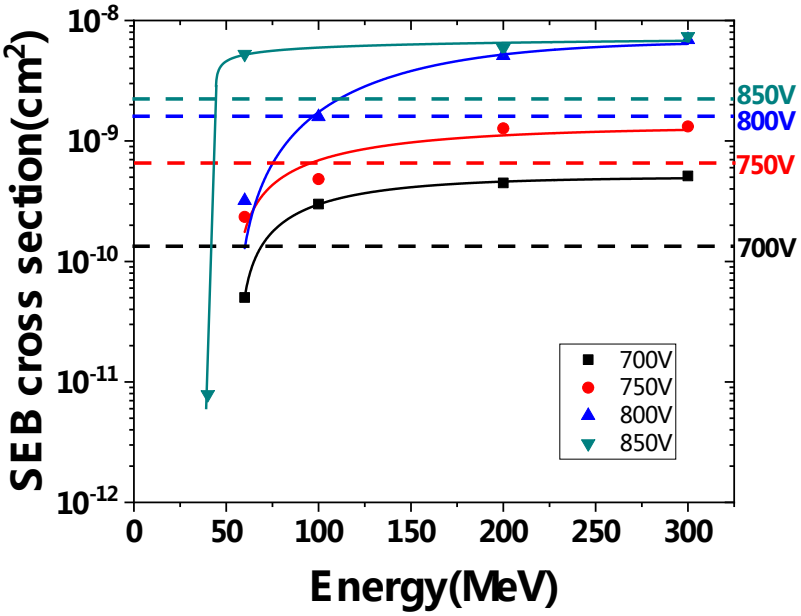

Fig. 4. SEB cross-sections as a function of proton energies under different drain biases for SiC power MOSFETs. The solid line is the Weibull fits of SEB cross-sections as a function of proton energies. The dash line shows the average SEB cross-section of the spallation neutron source under different drain biases.

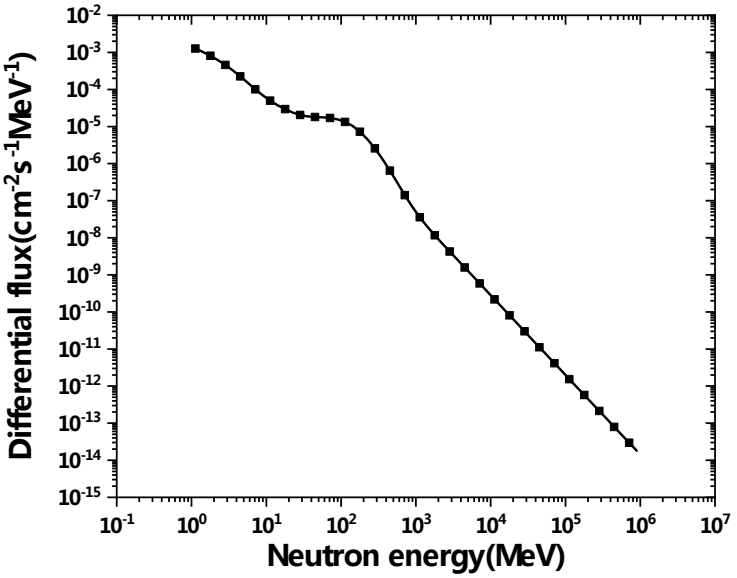

Fig. 5. Atmospheric neutron spetrum at New York sea level.

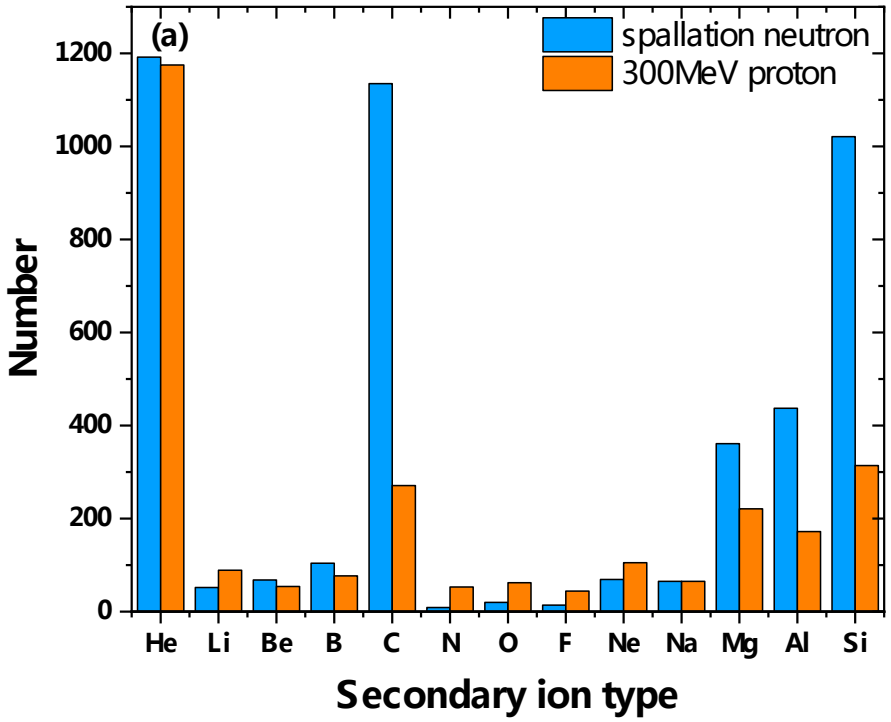

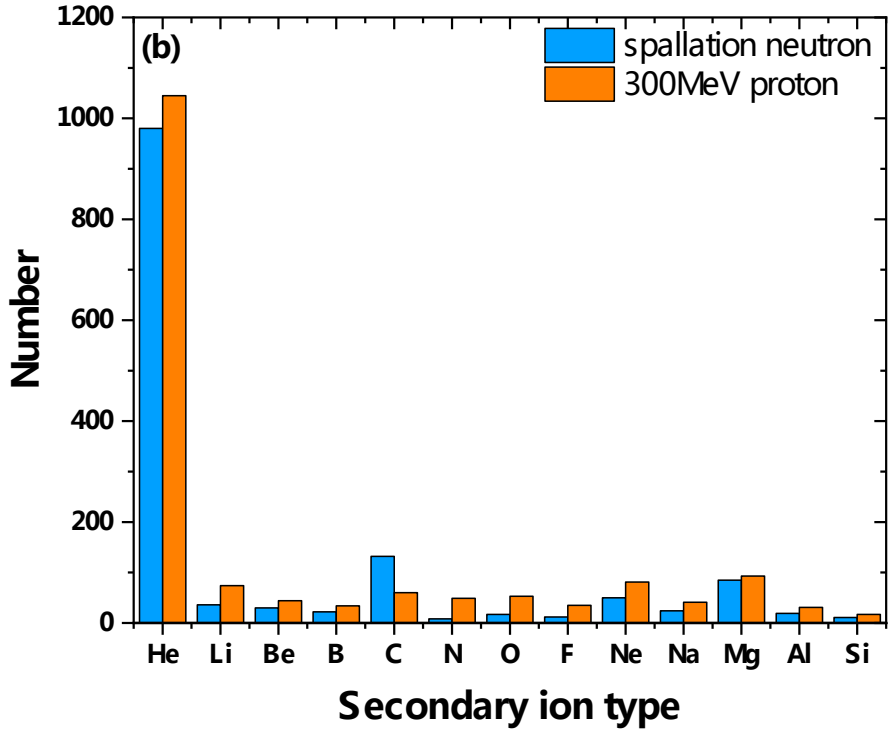

Fig. 6. (a) Number of all secondary ions produced by 300 MeV proton and spallation neutron. (b) Number of secondary ions with energy above 2 MeV produced by proton and spallation neutron.

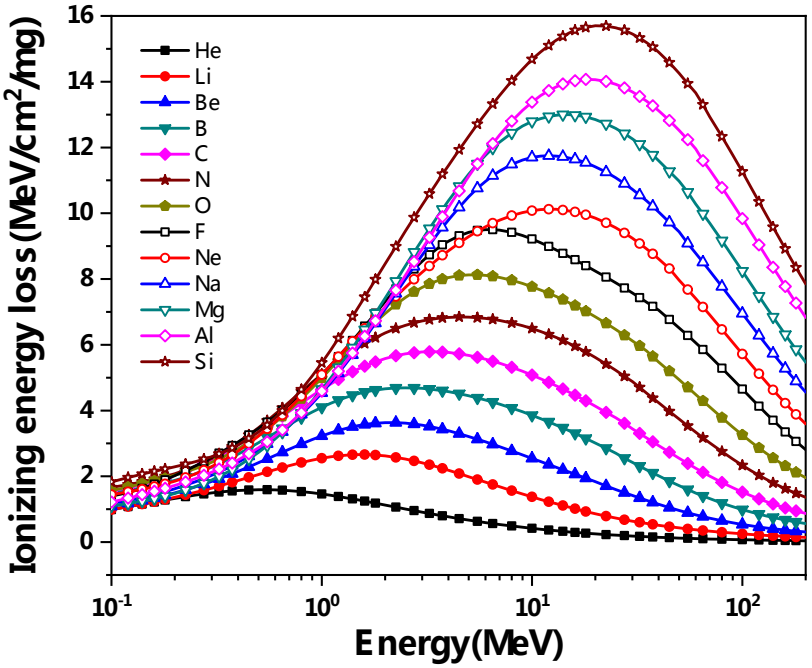

Fig. 7. Ionizing energy loss of different secondary ion as a function of energy.

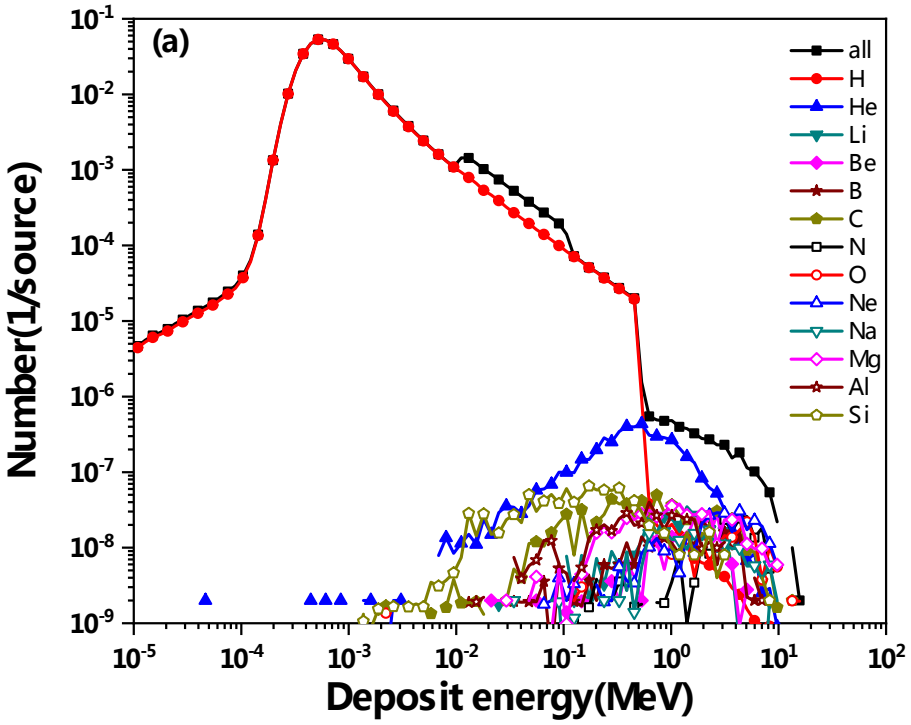
(a)
Number(1/source)
Deposit energy(MeV)
all
H
He
Li
Be
B
C
N
O
Ne
Na
Mg
Al
Si

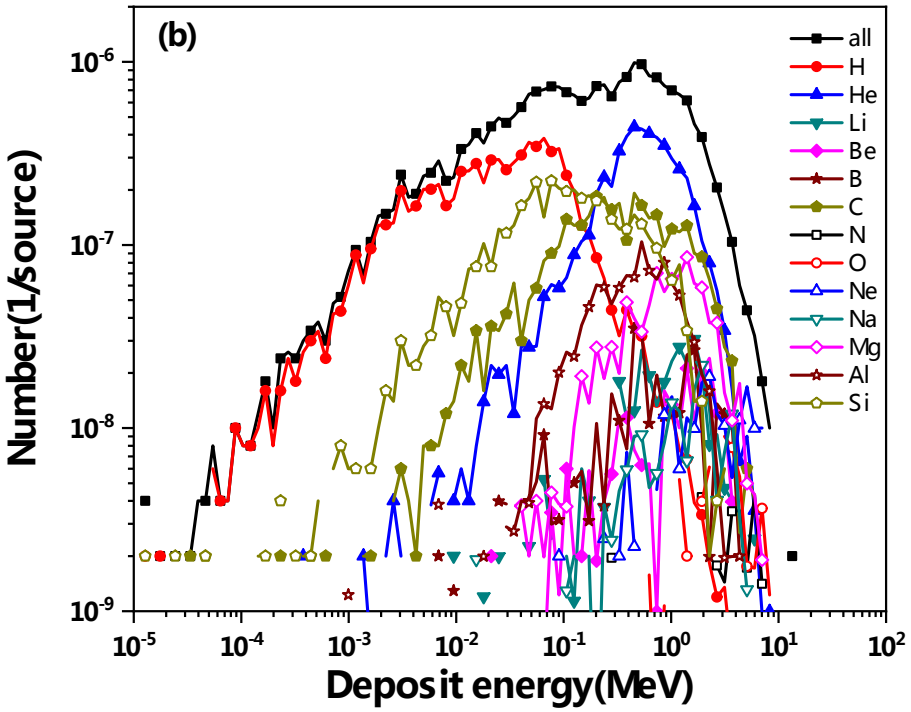
(b)
Number(1/source)
Deposit energy(MeV)
all
H
He
Li
Be
B
C
N
O
Ne
Na
Mg
Al
Si

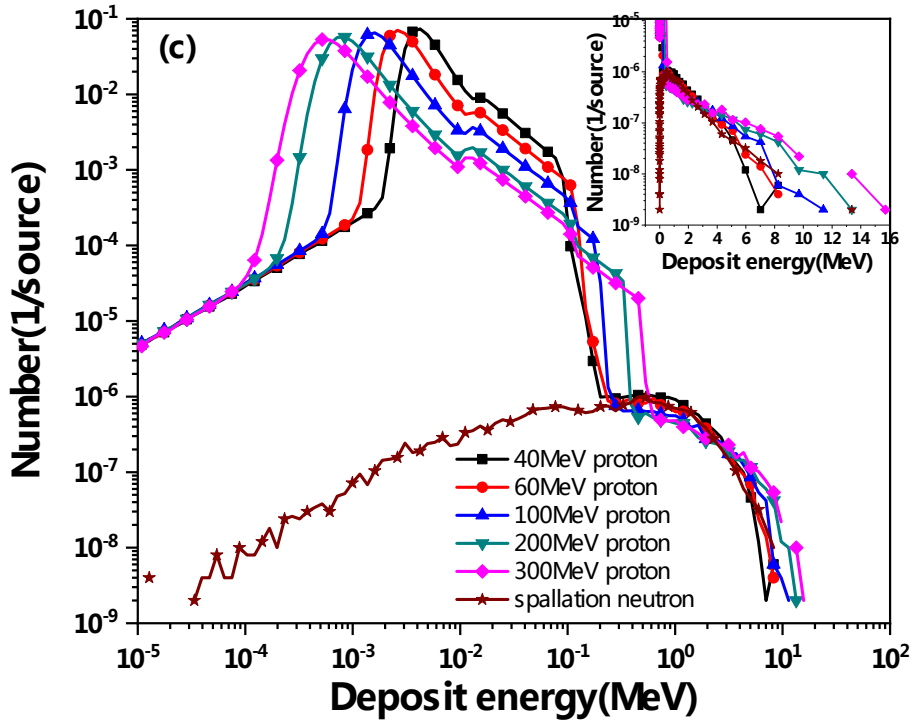

Fig. 8. (a) Deposit energies of different ions in SiC device for 300 MeV proton. (b) Deposit energies of different secondary ions in SiC device for spallation neutron. (c) Number of secondary ions produced by protons with different energies and spallation neutron as a function of deposit energy in SiC device.

Tab. 1. SEB cross-sections corresponding to different drain voltages under mono-energetic proton and spallation neutron irradiation

V_{ds} (V)	SEB cross-section(cm^2)					
	40 MeV proton	60 MeV proton	100 MeV proton	200 MeV proton	300 MeV proton	Spallation neutron
700	/	5.02×10^{-11}	3.00×10^{-10}	4.48×10^{-10}	5.12×10^{-10}	1.13×10^{-10}
750	/	2.34×10^{-10}	4.83×10^{-10}	1.27×10^{-9}	1.32×10^{-9}	6.67×10^{-10}
800	/	3.19×10^{-10}	1.59×10^{-9}	5.10×10^{-9}	6.92×10^{-9}	1.65×10^{-9}
850	7.86×10^{-12}	5.26×10^{-9}	/	5.87×10^{-9}	7.37×10^{-9}	2.04×10^{-9}

Tab. 2. Weibull fitting parameters corresponding to different drain biases

V_{ds} (V)	σ_0 (cm^2)	E_0 (MeV)	W	S
700	5.00×10^{-10}	56.31	49.05	0.87
750	1.31×10^{-9}	54.16	65.67	0.80
800	6.67×10^{-9}	53.21	109.20	1.42
850	8.11×10^{-9}	44.19	14.02	0.21

Tab. 3. Comparisons of SEB failure rates obtained by mono-energetic proton and spallation neutron irradiation under different drain voltages

V_{ds} (V)	SEB rate obtained by proton irradiation, $\lambda_{SEB,proton}$ (FIT)	SEB rate obtained by spallation neutron irradiation, $\lambda_{SEB,neutron}$ (FIT)	Error, $(\lambda_{SEB,proton}-\lambda_{SEB,neutron})/\lambda_{SEB,proton}$
700	2.73	1.47	46.2%
750	6.68	8.67	-29.8%
800	26.5	21.5	18.9%
850	52.0	26.5	49.0%